

Article

A State of Charge Estimator Based Extended Kalman Filter Using an Electrochemistry-Based Equivalent Circuit Model for Lithium-Ion Batteries

Xin Lai * , Chao Qin, Wenkai Gao, Yuejiu Zheng * and Wei Yi

School of Mechanical Engineering, University of Shanghai for Science and Technology, Shanghai 200093, China; Qin_Chao1995@126.com (C.Q.); wenkai_gao@163.com (W.G.); 13072182082@163.com (W.Y.)

* Correspondence: laixin@usst.edu.cn (X.L); yuejiu_zheng@163.com (Y.Z.); Tel.: +86-21-55275287 (Y.Z.)

Received: 22 August 2018; Accepted: 6 September 2018; Published: 8 September 2018



Abstract: In this paper, an improved equivalent circuit model (ECM) considering partial electrochemical properties is developed for accurate state-of-charge (SOC). In the proposed model, the solid-phase diffusion process is calculated by a simple equation about particle surface SOC, and the double layer is simulated by two resistance-capacitance (RC) networks. To improve the global accuracy of the model, a subarea parameter-identification method based on particle swarm optimization is proposed, in order to determine the optimal model parameters in the entire SOC area. Then, an SOC estimator is developed based on extended kalman filter. The comparative study shows that a model considering solid-phase diffusion with two RC networks is the best choice. Finally, experimental results show that the accuracy of the proposed model is one times higher than that of the traditional ECM in the low SOC area, and is able to estimate SOC with errors less than 1% in the entire SOC area. Furthermore, estimation results of two types of batteries under two working conditions indicate that the developed model and SOC estimator have satisfactory global accuracy and guaranteed robustness with low computational complexity, which can be applied in real-time situations.

Keywords: lithium-ion batteries; simplified electrochemical model; state of charge estimator; extended kalman filter

1. Introduction

Electrochemical energy storage systems (EESS) are power sources for many devices, e.g., cell phones, laptops, medical devices, electric vehicles (EVs), smart grid systems, etc. [1]. With a high demand of superior EESS, lithium-ion batteries (LIBs) have gained increasing popularity over other existing typical electrochemical batteries due to their favorable performances in high energy density, lightweight, long cyclic lifetime, low self-discharge rate, and almost zero memory effect [2,3]. However, LIB is a nonlinear dynamic system with a very narrow operating range, and some incorrect operations could lead to irreversible damage and shortened life [4–6]. Therefore, a reliable and effective battery management system (BMS) is required to optimize performance, improve safety and prolong life of LIBs. The critical state estimation, such as state of charge (SOC), state of health, and state of power, is fundamental in a BMS. Specifically, the SOC is an essential indicator used to regulate the operating decisions and to avoid overcharge or overdischarge [7]. However, the SOC cannot be directly measured by sensors, and the battery itself is highly nonlinear, which makes accurate SOC estimation very difficult [8].

1.1. Literature Review

Since the SOC estimation is essentially based on the battery model for most SOC estimation methods, an accurate battery model and matched model parameters are the prerequisite for accurate SOC estimation. Obviously, model accuracy is closely related to model structure and model parameter identification algorithm. The equivalent circuit models (ECMs) are the most common battery models adopted in the actual BMS because of few computations and acceptable precision [9]. The popular and widely reported ECMs include the Rint model, Thevenin model, partnership for a new generation of vehicles (PNGV) model, and general nonlinear (GNL) model [10–12], which are all based on resistance-capacitance (RC) networks with different orders. The model structure and electronic component values of the ECM directly affect the features and accuracy of the model. Ref. [13] investigated eleven ECMs and stated that the second-order RC models are the best choice owing to their balance of accuracy and reliability. However, ECMs are not empirical models, which means the model parameters have no clear electrochemical meaning [14]. Therefore, the model errors may be large, especially in low SOC area (SOC lower than 20%) [15]. Generally, the empirical model needs large computations and memories due to its complex equations, and currently it is still hard to use in a BMS for on-line estimation and real-time control. Based on the structure of ECM, Ref. [15] proposed an extended equivalent circuit model (EECM) considering partial electrochemical properties. However, the reliability of parameter identification is doubtful because nine parameters need to be identified in proposed EECM.

The most popular existing approaches for parameter identification of ECMs include the genetic algorithm (GA) [16], particle swarm optimization (PSO) algorithm [17], and the least-squares method [18]. The appropriate identification algorithm should match the battery model to pursue the balance between accuracy and computation. Moreover, the local optimization problem should also be avoided in the process of model parameter identification.

We could conclude that an improved ECM considering partial electrochemical properties is a better choice to balance accuracy and computational burden for online application. Moreover, appropriate model parameter identification and SOC estimation algorithm are essential for improving the accuracy and robustness of SOC estimation.

1.2. Main Contributions

This paper aims at developing an onboard battery model considering partial electrochemical properties and an accurate and robust SOC estimator in the entire SOC area. The unique contributions brought about in this paper are the following.

- (1) Four typical ECMs and four improved ECMs considering partial electrochemical properties are compared under the new European Driving Cycle (NEDC) and the dynamic stress test (DST) working conditions to obtain a more suitable battery model for the entire SOC area.
- (2) A subarea parameter-identification method based on PSO is proposed to improve the global model accuracy in the entire SOC area.
- (3) A SOC estimator based on extended kalman filter (EKF) for our proposed model is developed, and its accuracy and robustness are verified by experiments.

1.3. Organization of the Paper

The rest of this paper is organized as follows: Section 2 describes the developed model. In Section 3, a model-parameter identification method in the entire SOC area is proposed, and model errors are compared for various models to obtain a more appropriate model. Section 4 describes an EKF-based SOC estimator for the developed model, and its advantages are verified by experiments. Finally, conclusions drawn and the closing remarks are presented in Section 5.

2. Electrochemistry-Based Equivalent Circuit Model

2.1. Single-Particle Model

The pseudo-two-dimensional model (P2D) are widely used to describe the electrochemical behavior of lithium-ion batteries [14,19,20]. However, P2D is hard to use in onboard cases because of its complexity. Therefore, a series of model simplification attempts were made to reduce the computational complexity. The single-particle model (SPM) is a simplified model that is derived by approximating the electrode by a single spherical particle, and is becoming a popular model in recent years for SOC estimation [21,22]. The schematic of the SPM, which is illustrated in Figure 1.

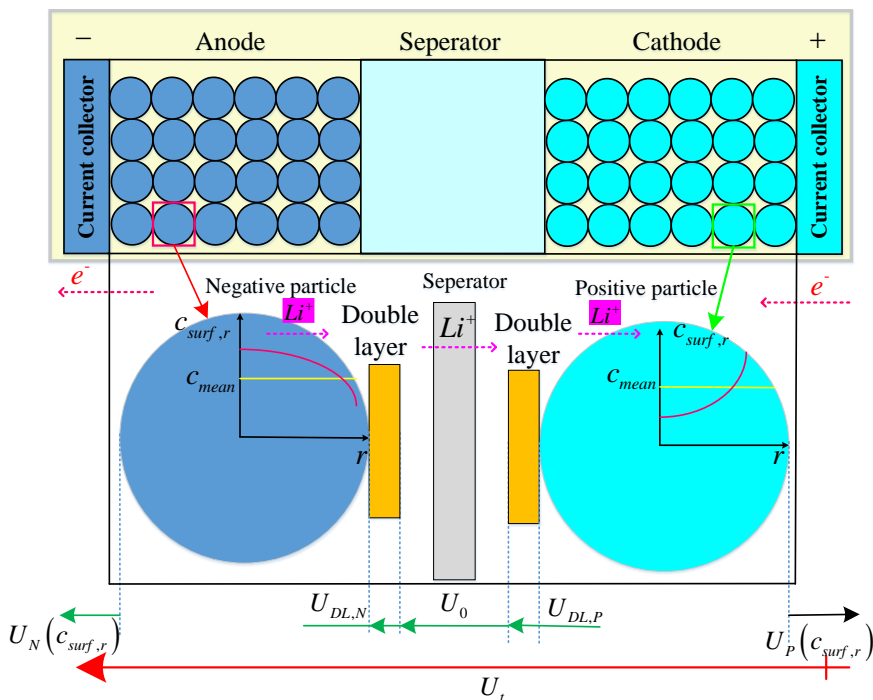


Figure 1. Schematic of the single-particle model (SPM) (modified from Reference [23]).

Based on Reference [15], the terminal voltage (U_t) can be expressed as:

$$U_t = (U_P(c_{surf,r}) - U_N(c_{surf,r})) - U_0 - U_{DL} \quad (1)$$

where $c_{surf,r}$ is lithium concentration at electrode particle surface, $U_P(c_{surf,r})$ and $U_N(c_{surf,r})$ are the surface potential of positive electrode and negative electrode, respectively. U_0 is the sum of the liquid phase voltage drop caused by the separator and electrolyte, and the voltage drop of the collector. U_{DL} is the voltage drop of the double layer, and it can be determined as:

$$U_{DL} = IR_{CT} \left(1 - e^{\left(\frac{-t}{\tau_{DL}} \right)} \right) \quad (2)$$

where R_{CT} is the resistance of the double layer, and τ_{DL} is time constant.

Moreover, Equation (1) can be rewritten as:

$$U_t = (U_P(SOC_{surf,r}) - U_N(SOC_{surf,r})) - U_0 - U_{DL} \quad (3)$$

where $SOC_{surf,r}$ is the SOC at particle surface. However, $SOC_{surf,r}$ could not be directly determined, and it can be expressed as:

$$SOC_{surf,r} = SOC_{avg} + \Delta SOC \quad (4)$$

where SOC_{avg} is the average SOC, which is represented by the average concentration of Li^+ in the electrode particle (C_{mean}). ΔSOC is the difference between SOC_{avg} and $SOC_{surf,r}$, which is related to the difference of $c_{surf,r}$ and C_{mean} in solid-phase diffusion process. According to Reference [15], ΔSOC follows the Equation (5):

$$\Delta SOC = K_{SD} I_F \left(1 - e^{\left(\frac{-t}{\tau_{SD}} \right)} \right) \quad (5)$$

where K_{SD} is concentration difference parameter in solid diffusion, I_F is the faradaic current, and τ_{SD} is time constant.

When the traditional ECM is used for SOC estimation, the open circuit voltage (OCV) of the battery U_{OCV} is looked up by the SOC_{avg} with the OCV-SOC curve. However, SOC_{avg} could not reflect the solid-phase diffusion. In this study, we used $U_{OCV}(SOC_{surf})$ instead of $U_{OCV}(SOC_{avg})$, and Equation (3) is hence rewritten as:

$$U_t = U_{OCV}(SOC_{surf}) - U_0 - U_{DL} \quad (6)$$

It is noted that the difference between the surface concentration c_{surf} and the average concentration C_{mean} indicates the solid-phase diffusion results. c_{surf} reflects the dynamic process of lithium-ion, which indirectly reflects the process of solid-phase diffusion. SOC_{surf} is closely related to c_{surf} . Therefore, our model includes the solid phase diffusion process and is a simplified electrochemical model.

2.2. ECM Considering Electrochemical Properties

A typical ECM generally uses the RC network comprising resistors and capacitors to simulate the dynamic characteristics of the battery, and these ECMS with n RC-networks is called the n RC model hereafter. The terminal voltage of the battery determined by the Kirchhoff voltage law can be expressed as [13,24]:

$$U_t = U_{OCV}(SOC) - IR_0 - \sum_{i=1}^n R_i \left(1 - e^{-t/R_i C_i} \right) \quad (7)$$

where R_0 is ohmic resistance, I is charge or discharge current, R_i and C_i are the i -th polarization resistance and i -th polarization capacitance, respectively.

Comparing Equation (7) with Equation (6), we can see that the model equations are very similar, the small difference is that the Equation (7) uses the SOC_{avg} , while the Equation (6) uses the SOC_{surf} . Combining traditional ECM and considering the solid-phase diffusion process inside the battery, an electrochemistry-based ECM is developed, and the schematic of this model is shown in Figure 2. In this model, the RC network is used to simulate the influence of the double electric layer, and a simple equation is used to calculate the solid-phase diffusion process. The number of RC networks corresponds to the number of double electric layers. To clarify the effect of the double layer and solid-phase diffusion on the model accuracy, eight models are chosen for comparison, and their mathematical equations are shown in Table 1. In Table 1, n RC represents ECMS with n RC-networks, EnRC ($n = 0, 1, 2, 3$) represents ECMS considering electrochemical properties. Obviously, n is the number of electric double layers in the model. In Section 3, model parameters will be identified, and errors of eight models will be compared to choose the right model.

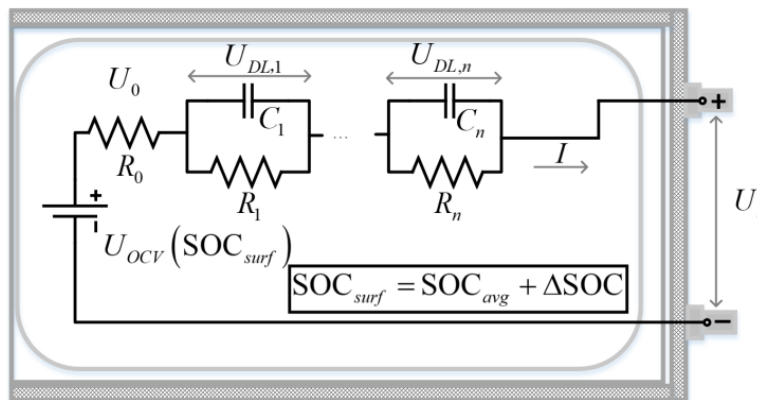


Figure 2. Schematic of the proposed EnRC model.

Table 1. Discretization equations of various resistance-capacitance (RC) models.

Model Name	Discretization Equations (Discharge Is Negative)	Number of Parameters
0RC	$U_t(k) = U_{OCV}(SOC_{avg}(k)) + IR_0$	2
E0RC	$\begin{cases} U_t(k) = U_{OCV}(SOC_{surf}(k)) + IR_0 \\ SOC_{surf}(k) = SOC_{avg} + \Delta SOC(k) \\ \Delta SOC(k) = \Delta SOC(k-1)e^{-\frac{T_s}{\tau_{SD}}} + K_{SD}I\left(1 - e^{-\frac{T_s}{\tau_{SD}}}\right) \end{cases}$	4
nRC: 1RC 2RC 3RC	$\begin{cases} U_t(k) = U_{OCV}(SOC_{avg}) + I_kR_0 + \sum_{i=1}^n U_i(k) \quad (n = 1, 2, 3) \\ U_i(k) = U_i(k-1)e^{-\frac{T_s}{\tau_i}} + I_kR_i\left(1 - e^{-\frac{T_s}{\tau_i}}\right) \end{cases}$	1RC: 4 2RC: 6 3RC: 8
EnRC: E1RC E2RC E3RC	$\begin{cases} U_t(k) = U_{OCV}(SOC_{avg}(k)) + I_kR_0 + \sum_{i=1}^n U_i(k) \quad (n = 1, 2, 3) \\ U_i(k) = U_i(k-1)e^{-\frac{T_s}{\tau_i}} + I_kR_i\left(1 - e^{-\frac{T_s}{\tau_i}}\right) \\ SOC_{surf}(k) = SOC_{avg} + \Delta SOC(k) \\ \Delta SOC(k) = \Delta SOC(k-1)e^{-\frac{T_s}{\tau_{SD}}} + K_{SD}I\left(1 - e^{-\frac{T_s}{\tau_{SD}}}\right) \end{cases}$	E1RC: 6 E2RC: 8 E3RC: 10

3. Model Parameter Identification and Comparison

3.1. Experiments

The experiments were performed using a commercial LIB with cathode of $LiNi_xCo_yMn_{1-x-y}$ (NCM). To fully verify the effectiveness of the proposed model, two types of LIBs were selected for experiments. The basic parameters of two LIBs are listed in Table 2. As shown in Figure 3a, the experiments were conducted in a battery tester made by DIGATRON which has a current range of -100 A to $+100$ A and a voltage range of 0 V to 20 V. The voltage accuracy is 1 mV and the current accuracy is $\pm 0.1\%$ full scale. A software (BTS-600, Digatron Power Electronics, Aachen, Germany) installed on PC is used to control the charging and discharging of the battery according to the given operating conditions, and record the terminal voltage and current of the battery at a frequency of 1 Hz. The acquired data was used for model parameter identification and SOC estimation.

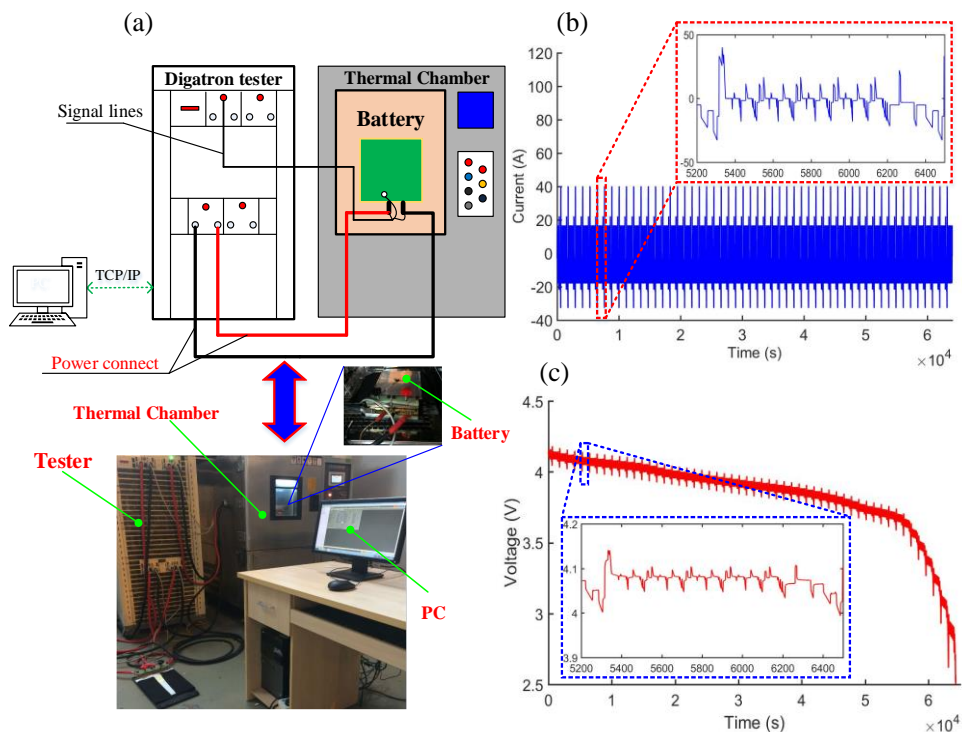


Figure 3. Experimental equipment and results. (a) Schematic of the cell test system; (b) Measured current under European Driving Cycle (NEDC) working condition; (c) Measured voltage under NEDC working condition.

Capacity and hybrid pulse power characterization (HPPC) experiments [25] were first performed to determine the capacity and OCV of LIBs. The capacity test process is as follows: Place the test LIB in the temperature chamber at 25 °C for 3 h. Then, discharge the LIB at a constant discharge current 1/3 C to 2.5 V. After waiting for 1 h, fully charge the LIB using the constant current-constant voltage (CC-CV) method. In this method, the LIB is charged at a constant current (1/3 C) until the voltage reaches 4.15 V, and then, the LIB is charged at a constant voltage until the charging current falls to 1.6 A; then, charging is paused for 1 h. This process is repeated three times, and the mean value of the test capacity is chosen as the battery capacity. The HPPC test is designed to determine the open circuit voltage (OCV). In this test, a series of pulse power sequences are provided to the fully charged battery. Following one pulse power sequence, the battery is discharged to a SOC of 97.5% at 1/3 C and rested for 3 h before the next pulse power sequence is provided. The battery is tested at decrements of 2.5% SOC (10% when the SOC is less than 90%) until the cutoff voltage of 2.5 V is reached.

Then, the two test LIBs were subsequently fully charged at 1/3 C. The discharge experiment was then performed, until the batteries were fully discharged at 1/3 C under the NEDC and DST working cycles until the cutoff voltage of 2.5 V is reached, respectively. It is noted that the charge and discharge currents are controlled by the program according to the cyclic working curve. The current and voltage curves under NEDC cycles on Cell #1 obtained from the experimental results are displayed in Figure 3b,c. The experimental data of Cell #2 under two cycle conditions are not listed here for brevity.

Table 2. Main parameters of experimental lithium-ion batteries (LIBs).

Type	Nominal Capacity (Ah)	Lower Cut-Off Voltage (V)	Upper Cut-Off Voltage (V)	Maximum Charge Current (A)
Cell #1	32.5	2.5	4.15	65
Cell #2	40	2.8	4.2	100

3.2. Model Parameter Identification Using PSO

For the n RC and EnRC, the model parameters that need to be identified and optimized can be expressed as:

$$\left\{ \begin{array}{l} V_j = \begin{bmatrix} R_0^+ & R_0^- \end{bmatrix} \text{ (if the model is 0RC)} \\ V_j = \begin{bmatrix} R_0^+ & R_0^- & \underbrace{\tau_1 & R_1}_{1st RC} & \underbrace{\tau_2 & R_2}_{2nd RC} & \cdots & \underbrace{\tau_n & R_n}_{n-th RC} \end{bmatrix} \text{ (if the model is } n\text{RC, } n = 1, 2, 3) \\ V_j = \begin{bmatrix} R_0^+ & R_0^- & \underbrace{\tau_1 & R_1}_{1st RC} & \underbrace{\tau_2 & R_2}_{2nd RC} & \cdots & \underbrace{\tau_n & R_n}_{n-th RC} & K_{SD} & \tau_{SD} \end{bmatrix} \text{ (if the model is EnRC)} \end{array} \right. \quad (8)$$

From Equation (8), it can be easily found that the identification parameters of the EnRC model are only two more than that of the n RC model. In the process of identification and optimization, the closer the model terminal voltage to the measured terminal voltage, the more accurate are the model parameters. Therefore, the root-mean-square error (RMSE) between the model terminal voltage and the measured terminal voltage can be employed as the fitness value to assess the model parameters and acquire the optimal model parameters that make the model voltage closest to the measured voltage. The objective function for the optimization can be expressed as:

$$\min : g(V) = \sqrt{\frac{1}{n} \sum_{k=1}^n (u_{i,k}(V) - \hat{u}_{i,k})^2}, \quad (9)$$

where $g(V)$ is the objective function, $u_{i,k}$ is the model voltage, and $\hat{u}_{i,k}$ is the measured voltage.

During parameter optimization, the upper and lower bounds of the parameters can be obtained by experimental results. The bounds of the same parameters for different models are maintained the same for fair comparison.

In this study, the PSO algorithm is used for global optimization for parameter identification of the above model. The PSO is a typical swarm intelligence algorithm, inspired by flocks of birds in search for food; it has been successfully applied for artificial neural-network training, function optimization, and pattern classification [26]. Because of the emergence of several variants over time, certain researchers have attempted to define a standard PSO version, with updates to incorporate the latest advances. The most recent standard PSO version was defined in 2011 and is referred to as the Standard PSO2011 (SPSO2011). The following is a brief description of the basic principles of PSO algorithm, and detailed descriptions of the PSO can be found in Reference [27].

Each particle in the algorithm represents a potential solution to the problem. The state of each particle is represented by its position x , velocity v , and fitness. In the iteration process, particle states are continuously updated until the termination criteria are met. Assume that in a D-dimensional search space, there is a swarm consisting of n particles, $\mathbf{X} = (X_1, X_2, \dots, X_n)$, where the velocity of the i th particle is expressed as a D-dimensional vector $\mathbf{X}_i = (X_{i1}, X_{i2}, \dots, X_{iD})^T$, the individual extremum is expressed as $\mathbf{P}_i = (P_{i1}, P_{i2}, \dots, P_{iD})^T$, and the swarm extremum is expressed as $\mathbf{P}_{best} = (P_{g1}, P_{g2}, \dots, P_{gD})^T$. Then, the following relationship exists between particle velocity and position update during the iteration process:

$$\mathbf{V}_{id}^{k+1} = \omega \mathbf{V}_{id}^k + c_1 r_1 (\mathbf{P}_{id}^k - \mathbf{X}_{id}^k) + c_2 r_2 (\mathbf{P}_{gd}^k - \mathbf{X}_{id}^k), \quad (10)$$

$$\mathbf{X}_{id}^{k+1} = \mathbf{X}_{id}^k + \mathbf{V}_{id}^{k+1}, \quad (11)$$

where ω is the inertia weight; $d = 1, 2, \dots, D$; $i = 1, 2, \dots, n$; k is the current iteration number; c_1 and c_2 are acceleration factors, and r_1 and r_2 are random numbers subject to uniform distribution within $[0, 1]$.

The calculation flow of PSO is shown in Table 3. Similar to other evolution-based algorithms, PSO is a random search algorithm. However, PSO preliminarily conducts a search based on its own velocity in order to avoid complex genetic operations; hence, it is a very efficient optimization algorithm.

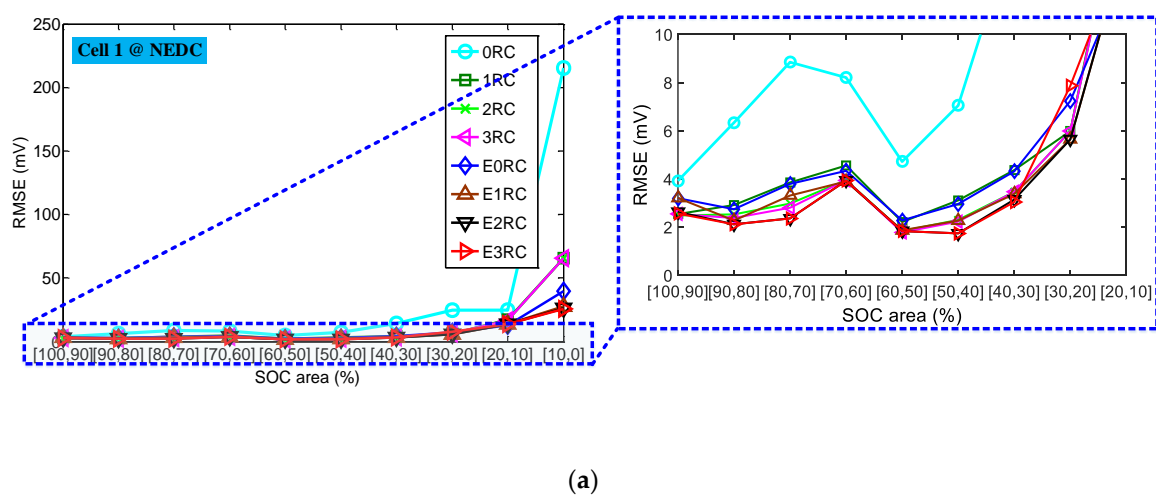
Table 3. Calculation flow of particle swarm optimization (PSO).

Step 1: Initialize the variables, randomly generate a particle swarm, and calculate the particle fitness values;
Step 2: Repeat the following steps until the termination criterion is satisfied (the error is sufficiently small, or the maximum loop count is reached):
Implement the following operations on each individual:
Update the velocity and position state (according to Equations (10) and (11));
Update the variable representing the individual's best position;
Step 3: Output the optimization results.

To improve the accuracy of the ECM in the entire SOC range, a subarea parameter-identification method is adopted in this study. The basic principles of this method are as follows: The entire SOC range (0–100%) is divided into 10 areas, and the PSO algorithm is then used to identify the model parameters in each area. Ten sets of model parameters are thereby obtained to form model parameters for the entire SOC area. For SOC estimation, the model parameters are selected based on the corresponding area of the SOC.

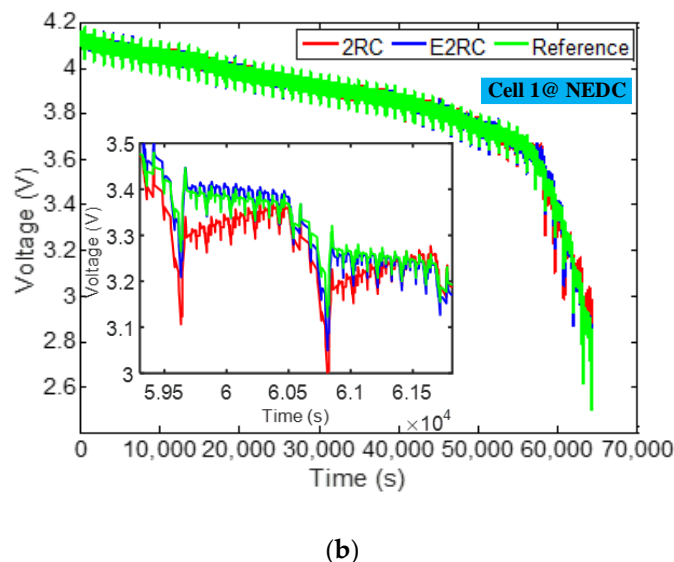
3.3. Results and Discussion

Model parameters of eight models are identified by the above method in the whole SOC area, and results are shown in Figures 4 and 5. Figure 4 shows identification results under NEDC working condition. As shown in Figure 4a, the accuracy of the EnRC model is obviously higher than that of the nRC model with the same order in the low SOC area, indicating that the proposed model provide satisfactory accuracy in the whole SOC area due to the consideration of the solid-phase diffusion process. Moreover, the model accuracy increases with the increase of the order of RC network, but it will not increase continuously. The accuracy of E2RC and E3RC models is almost the same. Therefore, the E2RC model is the best choice owing to its balance of accuracy and complexity. Figure 4b shows the estimated and measured terminal voltages of E2RC and 2RC models under NEDC working condition. Obviously, the model error of E2RC model is only half of that of 2RC model in the low SOC area. Table 4 lists the identification time of eight battery models, we can see that the computation time of our proposed model is slightly larger than that of the ECM with the same order. Through the above comparative analysis, we can conclude that E2RC model is the best choice with the best accuracy and low computation.



(a)

Figure 4. Cont.



(b)

Figure 4. Parameter identification results under NEDC working condition. (a) Root-mean-square error (RMSE) comparison for eight models; (b) terminal voltage profiles for 2RC and E2RC.

Table 4. Identification time of eight battery models (Cell 1@ European Driving Cycle (NEDC)) in the entire state-of-charge (SOC) area.

Model Name	Identification Time (s)
0RC	1.7796
E0RC	4.0983
1RC	5.2645
E1RC	5.9482
2RC	5.9897
E2RC	6.1520
3RC	8.5727
E3RC	11.3445

Figure 5 shows RMSE and terminal voltage comparisons of various models under DST working condition. We can see that the E2RC model is the best choice under DST. Based on the comparative study of the above eight models under two working conditions, we can conclude that the model error in the low SOC area is only half of that for traditional ECM, and the E2RC model is the most suitable model. Therefore, the battery model used in this study for SOC estimation is the E2RC model.

It is noted that the n in EnRC model represents the number of double layers in the SPM. It can be seen that the models with two double layers have the highest accuracy, which is consistent with the model shown in Figure 1. Moreover, the proposed model uses only one solid-phase diffusion equation in the SPM to achieve satisfactory model accuracy, which is different with the model proposed in Reference [14].

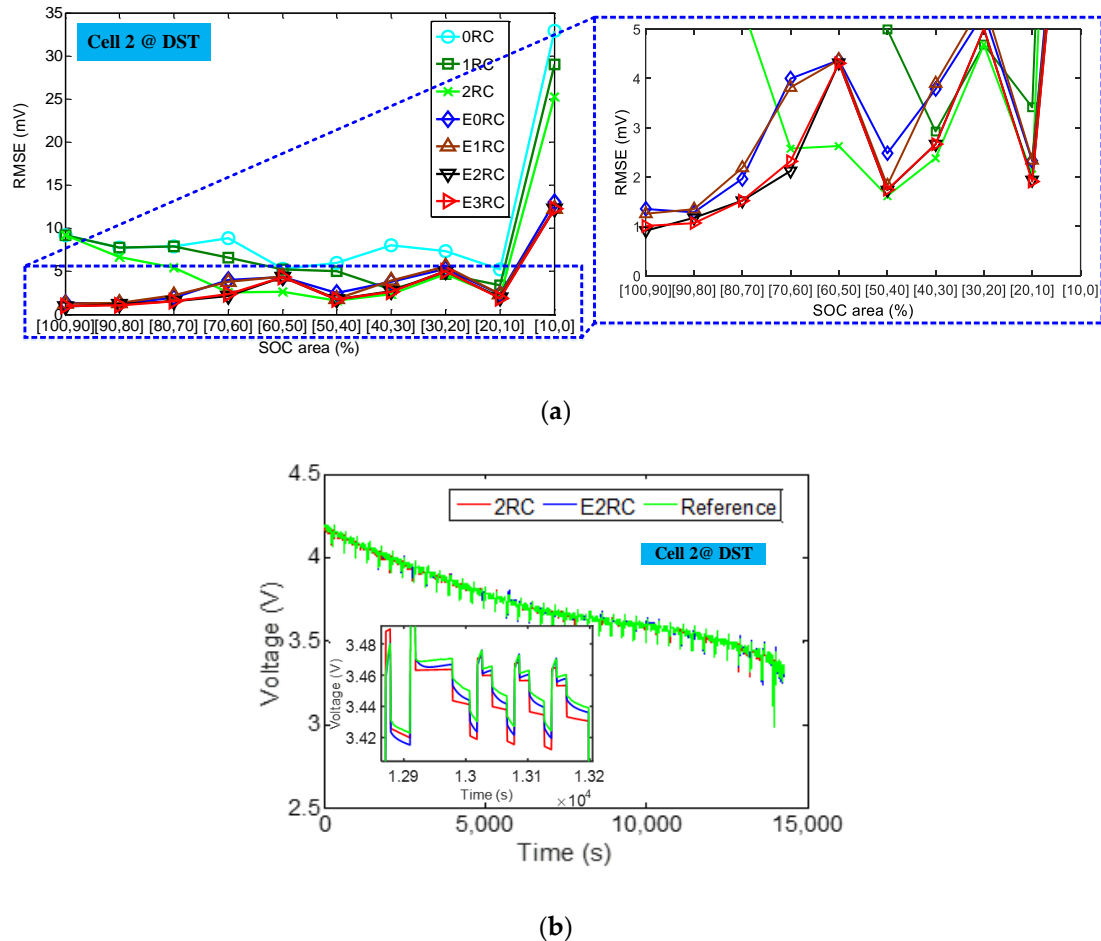


Figure 5. Parameter identification results under dynamic stress test (DST) working condition. (a) RMSE comparison; (b) Terminal voltage profiles for 2RC and E2RC.

4. SOC Estimation in the Entire SOC Area

4.1. EKF-Based SOC Estimator

The EKF algorithm is used to estimate the SOC in this paper. The EKF considers the noise characteristics of the current and voltage sensors, and effectively overcomes the problem of random errors [28]. The schematic of EKF is illustrated in Fig. 6. The EKF is based on dynamic equations. Assuming that k is the discrete-time index, \mathbf{x}_k is the state vector to be estimated, \mathbf{z}_k is the output vector, and the system input vector is \mathbf{u}_k . The battery model can be expressed by the following state equations:

$$\mathbf{x}_{k+1} = \mathbf{f}(\mathbf{x}_k, \mathbf{u}_k) + w_k \quad (12)$$

$$\mathbf{z}_k = \mathbf{h}(\mathbf{x}_k, \mathbf{u}_k) + v_k \quad (13)$$

where w_k denotes random process noise, v_k denotes measurement error, $\mathbf{f}(\mathbf{x}_k, \mathbf{u}_k)$ is a nonlinear state transition function, and $\mathbf{h}(\mathbf{x}_k, \mathbf{u}_k)$ is a nonlinear measurement function.

The state equations of the SOC estimator can be expressed as:

$$\mathbf{x}_k = (\text{SOC}_k, u_{1,k}, u_{2,k}, \Delta\text{SOC}) \quad (14)$$

$$\mathbf{h}_k = OCV(\text{SOC}_{surf,k}) - u_{1,k} - u_{2,k} - R_0 I_k + v_k \quad (15)$$

$$\mathbf{u}_k = I_k \quad (16)$$

In Figure 6, the superscript “−” and “+” indicate a priori estimate and a posteriori estimate at time step k , respectively. \mathbf{P} is the covariance matrix of uncertainty in state estimation; \mathbf{Q} is the covariance matrix of process noise; \mathbf{R} is covariance matrix for measuring uncertainty; $\bar{\mathbf{K}}_k$ is kalman gain matrix. The detailed EKF algorithm can be found in Reference [29].

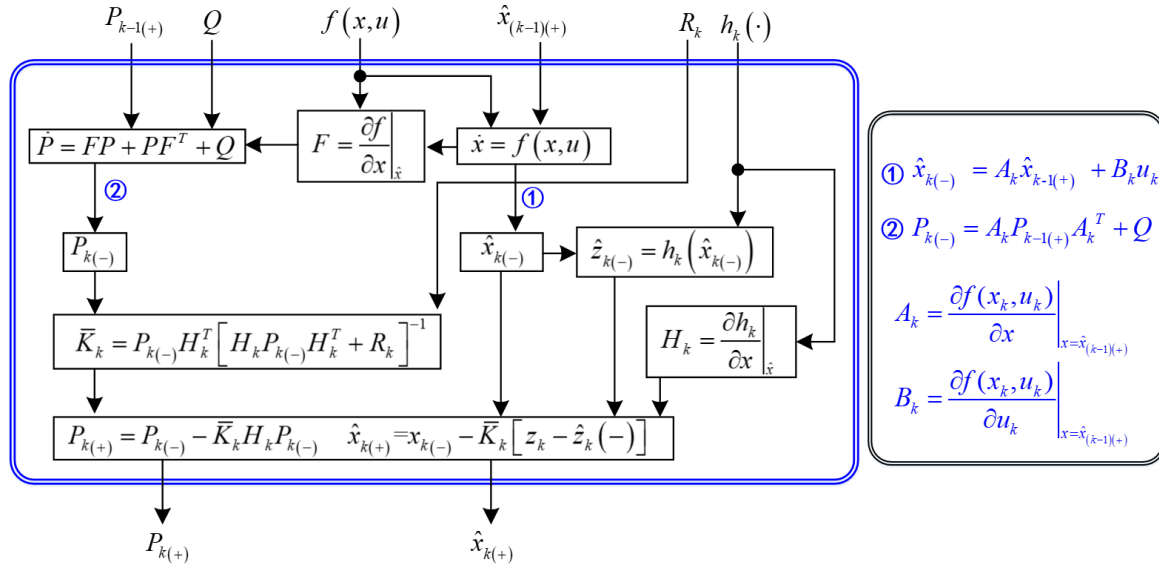


Figure 6. Schematic of extended kalman filter (EKF).

4.2. Results and Discussion

The EKF-based SOC estimator described in Section 4.1 is used to estimate the SOC under NEDC and DST working conditions in the entire SOC area (0–100%), respectively. The results are shown in Figures 7 and 8. Results imply that the SOC estimation error based on 2RC and E2RC model is similar in high SOC area, however, the SOC estimation error based on E2RC model is less 50% of that based on 2RC model in low SOC area. Moreover, the SOC estimation error based on E2RC model is always less than 1% in the entire SOC area.

Furthermore, in order to evaluate the robustness of our proposed model, we set various sensor errors and model errors to calculate the SOC estimation errors in the entire SOC area. The sensor error mainly originates from the voltage sensor and current sensor, whereas the model error has two types, namely, voltage drift or voltage noise. Reference [12] indicated that the voltage noise has no effect on the SOC error for a large time scale. Hence, the effect of the voltage drift (U_{drift}), model error (M_{drift}), and current sensor error (I_{drift}) on the SOC is considered in our study.

Figure 9 describes the influence of various model and sensor errors on the SOC estimated by EKF estimator under NEDC and DST working conditions. Figure 9a shows the relationship between the model error and the RMSE of SOC (R_{SOC}) based on E2RC model. We can see that as long as the M_{drift} is within $\pm 20mV$, R_{SOC} can be kept within 5%. Figure 9b shows the relationship between the U_{drift} and R_{SOC} . The U_{drift} is generally within 10 mV according to Reference [30]. In this case, R_{SOC} can be maintained at less than 3%. Figure 9b shows the relationship between the I_{drift} and R_{SOC} , indicating that I_{drift} has little effect on the R_{SOC} obtained by EKF estimator. From the above analysis, we can see that the proposed battery model can achieve satisfactory accuracy in a wide range of model and sensor errors, which implies that our proposed model has good robustness in the SOC entire area.

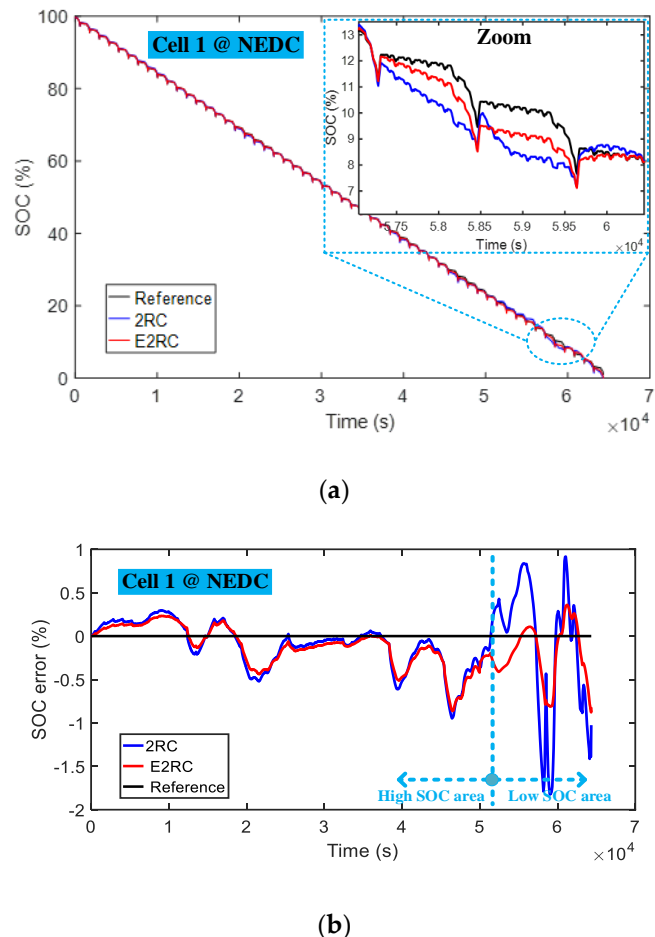


Figure 7. State-of-charge (SOC) estimation results under NEDC working condition. (a) SOC estimated value; (b) SOC error.

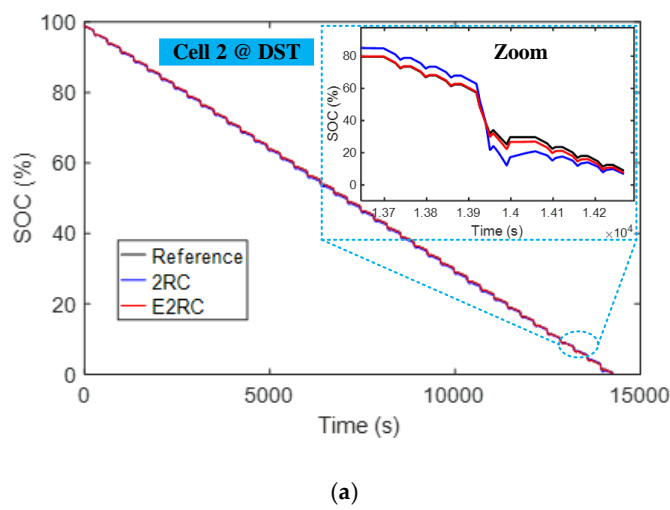


Figure 8. Cont.

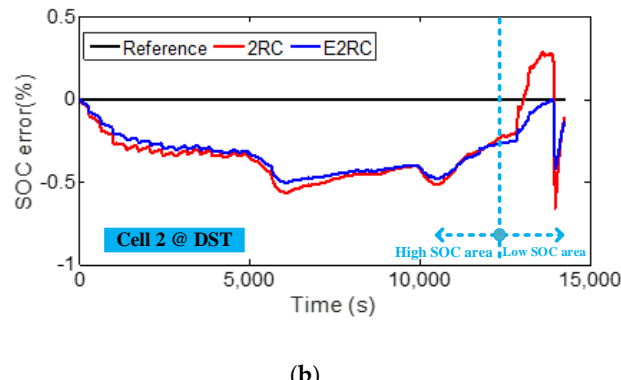


Figure 8. SOC estimation results under DST working condition. (a) SOC estimated value; (b) SOC error.

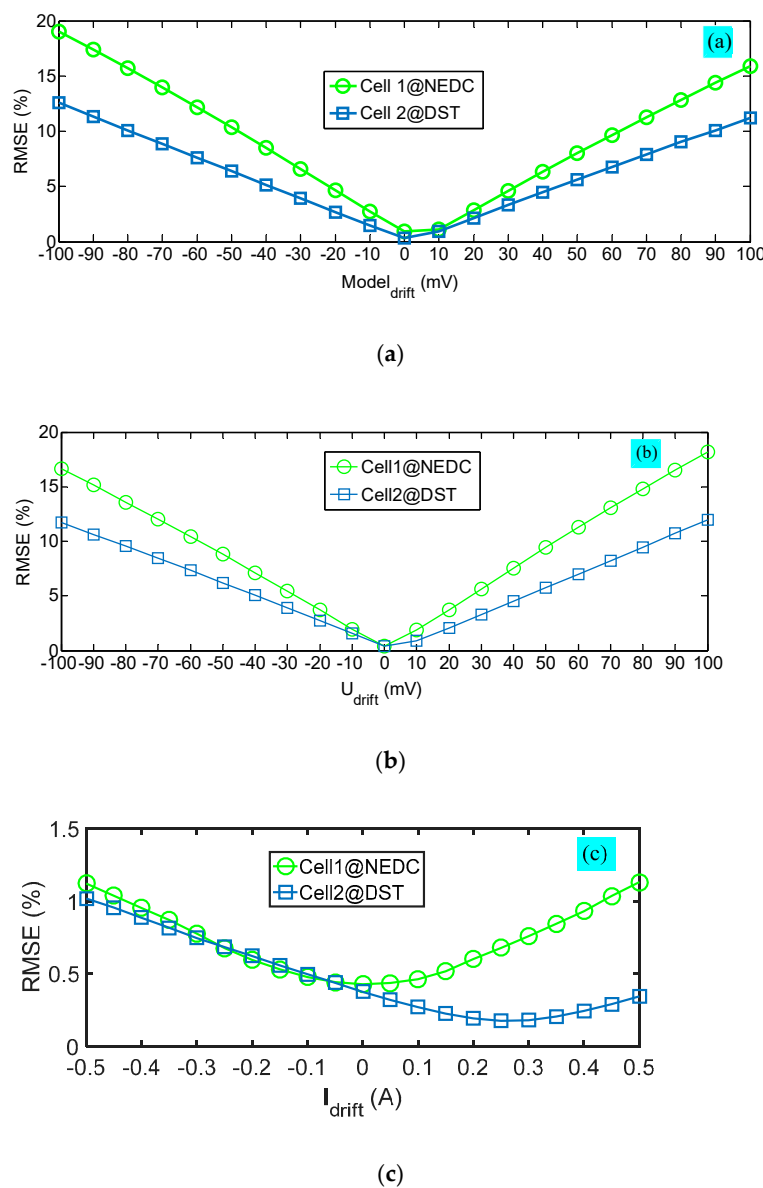


Figure 9. Influence of model and sensor errors on SOC estimated by EKF estimator under NEDC and DST working conditions. (a) Relationship between model error and SOC error. (b) Relationship between U_{drift} and SOC error. (c) Relationship between I_{drift} and SOC error.

5. Conclusions

This paper proposes a SOC estimator based on a SPM model in the entire SOC area. In this study, the PSO algorithm is employed to identify the global model parameters in the subarea, and the SOC estimation algorithm is estimated by EKF. The experimental results of two types of batteries under NEDC and DST conditions can be concluded as follows:

- (1) Comparative studies show that E2RC model is the best choice. The accuracy of the proposed model is one times higher than that of the traditional ECM in the low SOC area, and slightly better than that of the ECM in the high SOC area.
- (2) An EKF-based SOC estimator using our proposed model has higher SOC estimation accuracy than the ECM, especially in low SOC area. The SOC estimation error is less than 1% in the entire SOC area.
- (3) The proposed battery model and SOC estimation algorithm have satisfactory accuracy and robustness with low computational complexity.

Author Contributions: X.L. wrote the manuscript; X.L. and C.Q. conceived, designed and performed the experiments; W.Y. analyzed the data; W.G. contributed to the analysis of results; Y.Z. contributed to the analysis of results, provided feedback to the content and participated in writing the manuscript.

Funding: This research was funded by the National Natural Science Foundation of China (NSFC) under the grant number of 51505290 and 51507102.

Conflicts of Interest: The authors declare no conflict of interest.

References

1. Dong, G.Z.; Wei, J.W.; Chen, Z.H. Constrained bayesian dual-filtering for state of charge estimation of lithium-ion batteries. *Int. J. Electr. Power Energy Syst.* **2018**, *99*, 516–524. [[CrossRef](#)]
2. Zheng, Y.J.; Ouyang, M.G.; Han, X.B.; Lu, L.G.; Li, J.Q. Investigating the error sources of the online state of charge estimation methods for lithium-ion batteries in electric vehicles. *J. Power Sources* **2018**, *377*, 161–188. [[CrossRef](#)]
3. Chen, L.; Wang, Z.Z.; Lu, Z.Q.; Li, J.Z.; Ji, B.; Wei, H.Y.; Pan, H.H. A novel state-of-charge estimation method of lithium-ion batteries combining the grey model and genetic algorithms. *IEEE Trans. Power Electron.* **2018**, *33*, 8797–8807. [[CrossRef](#)]
4. Sahinoglu, G.O.; Pajovic, M.; Sahinoglu, Z.; Wang, Y.B.; Orlik, P.V.; Wada, T. Battery state-of-charge estimation based on regular/recurrent gaussian process regression. *IEEE Trans. Ind. Electron.* **2018**, *65*, 4311–4321. [[CrossRef](#)]
5. Ladpli, P.; Kopsaftopoulos, F.; Chang, F.K. Estimating state of charge and health of lithium-ion batteries with guided waves using built-in piezoelectric sensors/actuators. *J. Power Sources* **2018**, *384*, 342–354. [[CrossRef](#)]
6. Lai, X.; Zheng, Y.J.; Zhou, L.; Gao, W.K. Electrical behavior of overdischarge-induced internal short circuit in lithium-ion cells. *Electrochim. Acta* **2018**, *278*, 245–254. [[CrossRef](#)]
7. Wei, Z.B.; Zou, C.F.; Leng, F.; Soong, B.H.; Tseng, K.J. Online model identification and state-of-charge estimate for lithium-ion battery with a recursive total least squares-based observer. *IEEE Trans. Ind. Electron.* **2018**, *65*, 1336–1346. [[CrossRef](#)]
8. Chemali, E.; Kollmeyer, P.J.; Preindl, M.; Ahmed, R.; Emadi, A. Long short-term memory networks for accurate state-of-charge estimation of li-ion batteries. *IEEE Trans. Ind. Electron.* **2018**, *65*, 6730–6739. [[CrossRef](#)]
9. Panchal, S.; McGrory, J.; Kong, J.; Fraser, R.; Fowler, M.; Dincer, I.; Agelin-Chaab, M. Cycling degradation testing and analysis of a lifepo₄ battery at actual conditions. *Int. J. Energy Res.* **2017**, *41*, 2565–2575. [[CrossRef](#)]
10. Liu, C.Z.; Liu, W.Q.; Wang, L.Y.; Hu, G.D.; Ma, L.P.; Ren, B.Y. A new method of modeling and state of charge estimation of the battery. *J. Power Sources* **2016**, *320*, 1–12. [[CrossRef](#)]
11. He, H.W.; Xiong, R.; Guo, H.Q.; Li, S.C. Comparison study on the battery models used for the energy management of batteries in electric vehicles. *Energy Convers. Manag.* **2012**, *64*, 113–121. [[CrossRef](#)]
12. Ma, Y.; Duan, P.; Sun, Y.S.; Chen, H. Equalization of lithium-ion battery pack based on fuzzy logic control in electric vehicle. *IEEE Trans. Ind. Electron.* **2018**, *65*, 6762–6771. [[CrossRef](#)]

13. Lai, X.; Zheng, Y.J.; Sun, T. A comparative study of different equivalent circuit models for estimating state-of-charge of lithium-ion batteries. *Electrochim. Acta* **2018**, *259*, 566–577. [[CrossRef](#)]
14. Han, X.B.; Ouyang, M.G.; Lu, L.G.; Li, J.Q. Simplification of physics-based electrochemical model for lithium ion battery on electric vehicle. Part i: Diffusion simplification and single particle model. *J. Power Sources* **2015**, *278*, 802–813. [[CrossRef](#)]
15. Ouyang, M.G.; Liu, G.M.; Lu, L.G.; Li, J.Q.; Han, X.B. Enhancing the estimation accuracy in low state-of-charge area: A novel onboard battery model through surface state of charge determination. *J. Power Sources* **2014**, *270*, 221–237. [[CrossRef](#)]
16. Zhang, C.P.; Jiang, J.C.; Gao, Y.; Zhang, W.G.; Liu, Q.J.; Hu, X.S. Charging optimization in lithium-ion batteries based on temperature rise and charge time. *Appl. Energy* **2017**, *194*, 569–577. [[CrossRef](#)]
17. Tian, Y.; Li, D.; Tian, J.D.; Xia, B.Z. State of charge estimation of lithium-ion batteries using an optimal adaptive gain nonlinear observer. *Electrochim. Acta* **2017**, *225*, 225–234. [[CrossRef](#)]
18. Lim, K.; Bastawrous, H.A.; Duong, V.H.; See, K.W.; Zhang, P.; Dou, S.X. Fading kalman filter-based real-time state of charge estimation in lifepo₄ battery-powered electric vehicles. *Appl. Energy* **2016**, *169*, 40–48. [[CrossRef](#)]
19. Sturm, J.; Ennifar, H.; Erhard, S.V.; Rheinfeld, A.; Kosch, S.; Jossen, A. State estimation of lithium-ion cells using a physicochemical model based extended kalman filter. *Appl. Energy* **2018**, *223*, 103–123. [[CrossRef](#)]
20. Deng, Z.W.; Yang, L.; Deng, H.; Cai, Y.S.; Li, D.D. Polynomial approximation pseudo-two-dimensional battery model for online application in embedded battery management system. *Energy* **2018**, *142*, 838–850. [[CrossRef](#)]
21. Allam, A.; Onori, S. An interconnected observer for concurrent estimation of bulk and surface concentration in the cathode and anode of a lithium-ion battery. *IEEE Trans. Ind. Electron.* **2018**, *65*, 7311–7321. [[CrossRef](#)]
22. Meng, J.H.; Luo, G.Z.; Ricco, M.; Swierczynski, M.; Stroe, D.I.; Teodorescu, R. Overview of lithium-ion battery modeling methods for state-of-charge estimation in electrical vehicles. *Appl. Sci.* **2018**, *8*, 659. [[CrossRef](#)]
23. Liu, G.M.; Ouyang, M.G.; Lu, L.G.; Li, J.Q.; Han, X.B. Online estimation of lithium-ion battery remaining discharge capacity through differential voltage analysis. *J. Power Sources* **2015**, *274*, 971–989. [[CrossRef](#)]
24. Farmann, A.; Sauer, D.U. Comparative study of reduced order equivalent circuit models for on-board state-of-available-power prediction of lithium-ion batteries in electric vehicles. *Appl. Energy* **2018**, *225*, 1102–1122. [[CrossRef](#)]
25. Panchal, S.; Rashid, M.; Long, F.; Mathew, M.; Fraser, R.; Fowler, M. Degradation testing and modeling of 200 ah LiFePO₄ battery. *SAE Tech. Pap.* **2018**. [[CrossRef](#)]
26. Ma, Z.Y.; Wang, Z.P.; Xiong, R.; Jiang, J.C. A mechanism identification model based state-of-health diagnosis of lithium-ion batteries for energy storage applications. *J. Clean Prod.* **2018**, *193*, 379–390. [[CrossRef](#)]
27. Altinoz, O.T.; Yilmaz, A.E.; Duca, A.; Ciuprina, G. Incorporating the avoidance behavior to the standard particle swarm optimization 2011. *Adv. Electr. Comput. Eng.* **2015**, *15*, 51–58. [[CrossRef](#)]
28. Lin, X.F. Theoretical analysis of battery soc estimation errors under sensor bias and variance. *IEEE Trans. Ind. Electron.* **2018**, *65*, 7138–7148. [[CrossRef](#)]
29. Wei, J.W.; Dong, G.Z.; Chen, Z.H.; Kang, Y. System state estimation and optimal energy control framework for multicell lithium-ion battery system. *Appl. Energy* **2017**, *187*, 37–49. [[CrossRef](#)]
30. Lu, L.G.; Han, X.B.; Li, J.Q.; Hua, J.F.; Ouyang, M.G. A review on the key issues for lithium-ion battery management in electric vehicles. *J. Power Sources* **2013**, *226*, 272–288. [[CrossRef](#)]



© 2018 by the authors. Licensee MDPI, Basel, Switzerland. This article is an open access article distributed under the terms and conditions of the Creative Commons Attribution (CC BY) license (<http://creativecommons.org/licenses/by/4.0/>).